RESEARCH ARTICLE
doi: 10.2306/scienceasia1513-1874.2022.121

ScienceAsia 48 (2022): **804–812**

Adsorption behavior and mechanism of alizarin yellow and rhodamine B dyes on water hyacinth (*Eichhornia crassipes*) leaves

Suchada Sawasdee*, **Prachart Watcharabundit**

Department of Chemistry, Thepsatri Rajabhat University, Lopburi 15000 Thailand

*Corresponding author, e-mail: ps_neng@hotmail.com

Received 10 Jan 2022, Accepted 30 May 2022
Available online 10 Aug 2022

ABSTRACT: This work studied a low-cost water hyacinth biosorbent to remove alizarin yellow (AY) and rhodamine B (RB) from aqueous solutions. The physicochemical characterization of the water hyacinth leaf (WHL) was carried out by Brunauer-Emmett-Teller surface area analysis, Fourier transform infrared spectroscopy, and scanning electron microscopy. Contact time, pH, initial dye concentration, and temperature on adsorption were investigated in batch mode. The maximum removal of AY and RB was detected at pH 2. The results showed that the adsorption of dyes was enhanced with increased contact time, initial dye concentration, and temperature. The contact time reached equilibrium within 120 min and 90 min for AY and RB, respectively. The Langmuir and Freundlich isotherm models were applied to the equilibrium data. The Langmuir isotherm model better described the equilibrium data, indicating the monolayer adsorption for all dyes. The maximum adsorption capacity values from the Langmuir model were 37.04 and 23.98 mg/g for AY and RB, respectively. The kinetic data of the adsorption were better described using the pseudo-second-order model. Thermodynamic studies showed that the adsorption of dyes was endothermic and spontaneous, and the adsorption was physisorption. The adsorption mechanisms involved H-bonding, Yoshida H-bonding, $n-\pi$, and $\pi-\pi$ interactions for both dyes. Moreover, electrostatic interactions could form between the negative parts of AY and the positive surface of the water hyacinth leaf. In conclusion, the water hyacinth leaf could be employed as a low-cost adsorbent to remove AY and RB from wastewater.

KEYWORDS: cationic dye, anionic dye, water hyacinth, adsorption mechanism

INTRODUCTION

Industries such as textiles, plastics, rubber, leather, cosmetics, and paper use many kinds of artificial composite dyes and discharge large volumes of colored wastewater, causing major environmental pollution problems. More than 10 000 types of dyes are commercially available with over 7×10^5 tons of dyestuff produced annually [1], and about 10% of the total is released into the environment [2]. Synthetic dyes usually have an aromatic molecular structure, making them non-biodegradable [3], and most dye molecules are difficult to degrade with light, heat, and chemicals [4]. Dyes give an undesirable color to the water and reduce light penetration and photosynthesis, causing severe problems for the ecosystem. The presence of dyes can cause damage to living organisms in the water.

Dyes are broadly categorized into cationic and anionic dyes, and the former is considered more toxic than the latter [5]. AY is an anionic azo dye with applications in textiles, leather, plastics, and pharmaceuticals. Direct contact with it is harmful to the gastrointestinal system and eyes [6]. RB is a highly water-soluble synthetic dye that belongs to the xanthene class. It is used in agate dying, the animal feed, and textile industries. RB irritates the skin, eyes, and respiratory tract and is implicated in causing carcinogenicity, reproductive and developmental neurotoxicity, and chronic toxicity to humans and animals [7].

Several methods have been used to remove these dyes from wastewater [1, 8]. From these techniques, adsorption is one of the most effective methods for removing dyes from wastewater. The method has broad applications in decolorization due to the economic cost, high efficiency, eco-friendliness, and inactivity towards toxic substances [9]. Recently, natural biosorbents have been the most popular choice for wastewater treatment due to their capacity, abundance, and relatively low cost. Some of the natural biomaterial adsorbents that have been used for the adsorption of dyes are rattan sawdust [10], cashew shells [11], coir pith [12], poplar leaves [4], breadnut peels [13], and *Moringa olifera* pod husks [14]. However, the search for an economical, eco-friendly, and highly effective adsorbent continues.

Water hyacinth creates dense mats of biomass on the water surfaces of canals and rivers; these mats cause problems including clogging irrigation facilities and water pollution. However, these mats can be used as an efficient and economical adsorbent for effluent, and their leaves can be used as a biosorbent to remove dyes such as methylene blue, Victoria blue [15], methyl red [16], amaranth dye [17], and metanil yellow [18]. The present study focuses on removing dyes from aqueous solution using water hyacinth leaves. In addition, this work evaluated the adsorption of AY (anionic dye) and RB (cationic dye) by WHL, and the adsorption mechanism was discussed.

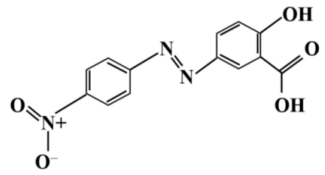

Alizarin yellow (AY)

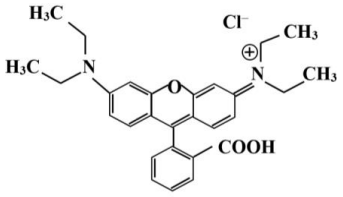

Rhodamine B (RB)

Fig. 1 Chemical structures of AY and RB.

MATERIALS AND METHODS

Adsorbent preparation

Raw WHL were collected from a canal in the Banmi District, Lopburi Province, Thailand. They were washed with tap water and dried in a hot air oven at 80 °C. The dried adsorbent was powdered and sieved to a particle size of 150–300 mm and kept in a desiccator until used.

Adsorbate preparation

AY (CI 32602, $C_{13}H_9N_3O_5$, 287.23 g/mol, Riedel-de Haen, Germany) and RB (CI 83690, $C_{28}H_{31}ClN_2O_3$, 479.02 g/mol, Fluka, USA) were used as the adsorbates. The chemical structures of both dyes are shown in Fig. 1. For the experiments, various concentrations (50–500 mg/l) of dye solutions were prepared and diluted with distilled water. The pH of dye solutions was measured using an Ohaus pH meter, and the pH adjustments were made by adding 1 M HCl or 1 M NaOH.

Adsorbent characterization

The adsorbent used in this study was characterized by Brunauer-Emmett-Teller (BET) surface area analysis (Quantachrome, NovaWin, Autosorb 1 MP, USA), Fourier transform infrared (FTIR, Perkin Elmer, model two, USA) spectroscopy, and scanning electron microscope (SEM, LEO, model 1450 VP LEO, England).

Batch method of adsorption

Adsorption studies were performed using the batch method. For each experimental run, 100 ml of dye solution of known concentration was placed in a 250-ml Erlenmeyer flask containing 0.05 g and 1.00 g of adsorbent for AY and RB adsorption, respectively. The flasks containing the suspended mixture were agitated at constant temperature and a shaking rate of 200 rpm within a temperature-controlled orbital shaker. At the appropriate time intervals, each sample was withdrawn and filtered. The supernatant was measured for dye concentration using a UV-Visible spectrophotometer (Analytik Jena, Specord 210 plus, Germany) at 370 and 554 nm for AY and RB, respectively. The adsorption capacity (q_t) was calculated by [5]:

$$q_t = \frac{(C_0 - C_t)V}{W} \tag{1}$$

where C_0 (mg/l) is the initial dye concentration of adsorbent, C_t (mg/l) is the concentration remaining in the solution at time t (min), q_t (mg/g) is the amount adsorbed at any time, V (l) is the volume of the solution, and W (g) is the mass of the adsorbent. All the experiments were carried out in triplicate under identical conditions, and each average value was calculated for further use.

Adsorption isotherm

Adsorption isotherms can describe the distribution of the dye molecules between the adsorbent and dye solution at equilibrium. This study tested the experimental data using the Langmuir and Freundlich isotherm models.

The Langmuir is represented in a linear form as follows [13]:

$$\frac{C_e}{q_e} = \frac{1}{q_{\max}} C_e + \frac{1}{K_L q_{\max}} \tag{2}$$

where C_e (mg/l) is the equilibrium concentration, q_e (mg/g) is the adsorption capacity at equilibrium, K_L is the Langmuir constant, and $q_{\max}$ (mg/g) is the maximum adsorption capacity. The dimensionless separation factor of the Langmuir isotherm, R_L , is defined by [13]:

$$R_L = \frac{1}{1 + K_L C_0} \tag{3}$$

where R_L values indicate the adsorption to be unfavorable when $R_L > 1$, linear when $R_L = 1$, favorable when $0 < R_L < 1$, and irreversible when $R_L = 0$.

The Freundlich isotherm is represented in a linear form as follows [13]:

$$\log q_e = \log K_F + (1/n) \log C_e \tag{4}$$

where K_F (l/g) is the Freundlich constant, and $1/n$ is the adsorption intensity.

Adsorption kinetics

Kinetic studies are necessary to understand the adsorption mechanism. This is because adsorbate molecules undergo different steps when they transfer from the bulk solution to the adsorbent surface. These steps include the migration of adsorbate molecules to the

exterior surface of adsorbent particles and pore diffusion [19]. Typically, 3 kinetic models — pseudo-first-order, pseudo-second-order, and intraparticle diffusion — were used to explain adsorption.

The pseudo-first-order and pseudo-second-order kinetic models in the linear form are written as [5]:

$$\log(q_e - q_t) = \log q_e - \frac{k_1}{2.303} t \tag{5}$$

$$\frac{t}{q_t} = \frac{1}{k_2 q_e^2} + \frac{1}{q_e} t \tag{6}$$

where k_1 (min^{-1}) and k_2 ($\text{g}/(\text{mg}\cdot\text{min})$) are the rate constants of the pseudo-first-order and pseudo-second-order kinetic adsorption, respectively, q_e (mg/g) is the amount adsorbed at equilibrium, and q_t (mg/g) is the amount adsorbed at any time t (min).

The intraparticle diffusion model is written in the linear form as [5]:

$$q_t = K_{\text{id}}(t)^{1/2} + C \tag{7}$$

where K_{id} is the rate constant of the intraparticle diffusion model, and C is the thickness of the boundary layer.

Adsorption thermodynamics

The Gibbs free energy change (ΔG°) of the adsorption process can be expressed as Eq. (8) [11]:

$$\Delta\text{G}^\circ = -RT \ln K_c \tag{8}$$

where K_c is the equilibrium adsorption constant, R is the gas constant, and T is the absolute temperature. The enthalpy (ΔH°) and entropy (ΔS°) changes can be estimated using Eq. (9) [11]:

$$\Delta\text{G}^\circ = \Delta\text{H}^\circ - T\Delta\text{S}^\circ. \tag{9}$$

ΔH° and ΔS° can be determined from the intercept and slope of the plot of ΔG° against T.

RESULTS AND DISCUSSION

Adsorbent characterization

The nitrogen adsorption-desorption isotherm of WHL was investigated, and the results of the BET analysis are shown in Table 1. The isotherm was type III with a hysteresis loop. As seen in Table 1, the specific surface area of the WHL was 11.134 m^2/g with a total pore volume of 0.019 cm^3/g and an average pore radius of 3.471 nm. Under IUPAC classification, the pores of materials are classified into 3 groups: micropore (< 2 nm), mesopore (2–50 nm), and macropore (> 50 nm). Because the pore size diameter of the WHL was 6.826 nm, the pores were classified as mesopores.

The FTIR spectra of WHL before and after adsorption are presented in Fig. 2. Prior to adsorption (Fig. 2a), the peaks at 3303.3 and 2924.6 cm^{-1} were due to —OH and —CH stretching, respectively. The peak at 1730.9 cm^{-1} was assigned to the carbonyl (C=O) group. The peak at 1600.6 cm^{-1} corresponded to the C=C stretching of aromatic groups that may be attributed to the hemicelluloses and lignin aromatic groups [20]. The peak in the 1300–1420 cm^{-1} range was due to C=C—H in-plane bending associated with cellulose [2]. The bands between 1320 and 1210 cm^{-1} may be due to the axial deformation vibrations of the C—O bond in phenol [21]. The peak observed at 1027.3 cm^{-1} was due to C—O stretching, while the peaks at 1319.1 and 1371.3 cm^{-1} indicated C—H bending [22]. The peak at around 1027 cm^{-1} was the C—O—C pyranose ring stretching vibration [23]. The peaks shifted to other frequencies after adsorption (Fig. 2b,c). For example, the peak at 1600.6 cm^{-1} shifted to a higher frequency, and the peak at 1319.1 cm^{-1} shifted to a lower frequency. Moreover, the intensities of the peaks following adsorption such as 3303.3, 1600.6, and 1027.3 cm^{-1} were lower than the pre-adsorption peaks due to the interaction between the dye molecules and functional groups on the surface of the adsorbent. In contrast, the peak intensities at 1730.9 cm^{-1} of the adsorption for both dyes were higher than the before adsorption peak due to an increase in the amount of the carbonyl (C=O) group of dye molecules.

Table 1 Surface area and pore size of adsorbent.

Parameter	WHL
BET surface area (m^2/g)	11.134
Total pore volume (cm^3/g)	0.019
Average pore radius (nm)	3.471
Dp (nm) (BET)	6.826

The surface morphology of the WHL before and after adsorption was characterized by SEM analysis, as shown in Fig. 3. Before adsorption, the adsorbent particles had pores with a high degree of heterogeneity. However, in the SEM images of the post adsorption WHL in Fig. 3(b,c), the adsorbent pores were covered with dyes, indicating the dye adsorption on the surface of the WHL.

Effects of pH

The pH of the solution is an important factor in the adsorption mechanism and the surface charge of the adsorbent. The effects of the pH (2–10) of the dye solution on the equilibrium uptake capacity were studied at 30 °C. Fig. 4 shows that the adsorption capacity of both dyes decreased with increased pH. The maximum adsorption capacity at pH 2 was 9.414 and 4.632 mg/g for AY and RB, respectively. The maximum adsorption at pH 2 was due to the formation of a layer of H^+ on the surface of the adsorbent and the negative parts of the nitro group of AY. RB, a positive dye molecule, could be adsorbed because it formed monomeric molecules

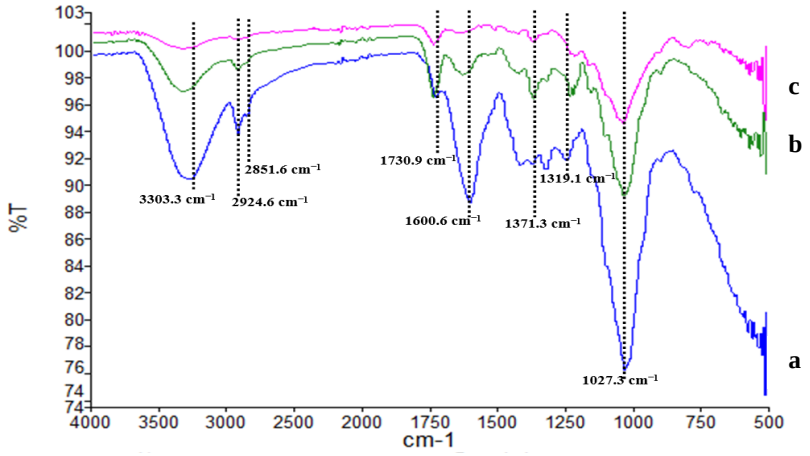

Fig. 2 FTIR of WHL before and after dye adsorption: (a) before adsorption, (b) after RB adsorption, and (c) after AY adsorption.

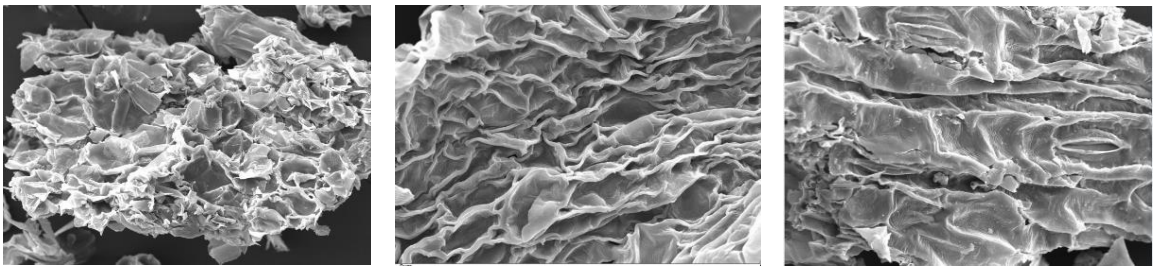

Fig. 3 SEM images of WHL: (a) before dye adsorption, (b) after RB adsorption, and (c) after AY adsorption.

and entered the pores of the adsorbent. At higher pH, more negatively charged surface sites were available, and the adsorption of AY decreased because of the repulsion. The zwitterionic form of RB in water may increase the aggregation of RB to generate a dimer, which is larger than the monomer, and the dimer is unable to enter the pore [24].

Effects of contact time and initial concentration

The effects of contact time on the adsorption of the dyes were investigated at 5 concentrations (50, 100, 200, 300, and 400 mg/l) of dyes (Fig. 5). The removal rate of dyes (AY and RB) increased rapidly initially and decreased gradually with time until equilibrium was reached at 120 min for AY and 90 min for RB. The initial rapid adsorption was due to the abundant number of active sites available on the surface of the absorbent.

Moreover, the adsorption increased with increase in the initial dye concentration. This effect may be due to the increased driving force of the concentration gradient for mass transfer. In this case, the dyes were mainly adsorbed on the exterior surface, and then they were adsorbed on the interior surface of the WHL. Similar findings have been observed for contact time and

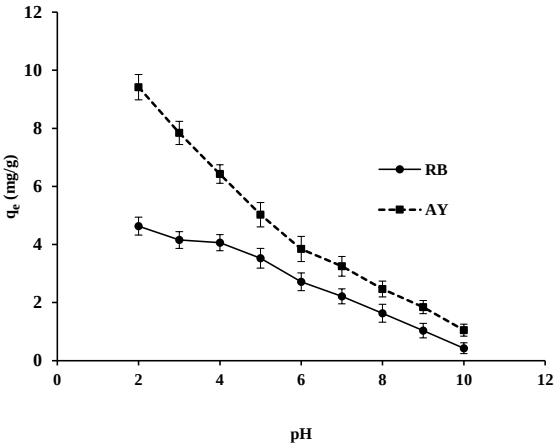

Fig. 4 The effects of pH on dye adsorption. Conditions: contact time 180 min, initial dye concentration of 50 mg/l, and adsorbent dose of 0.5 g for AY and 1.0 g for RB, at 30 °C.

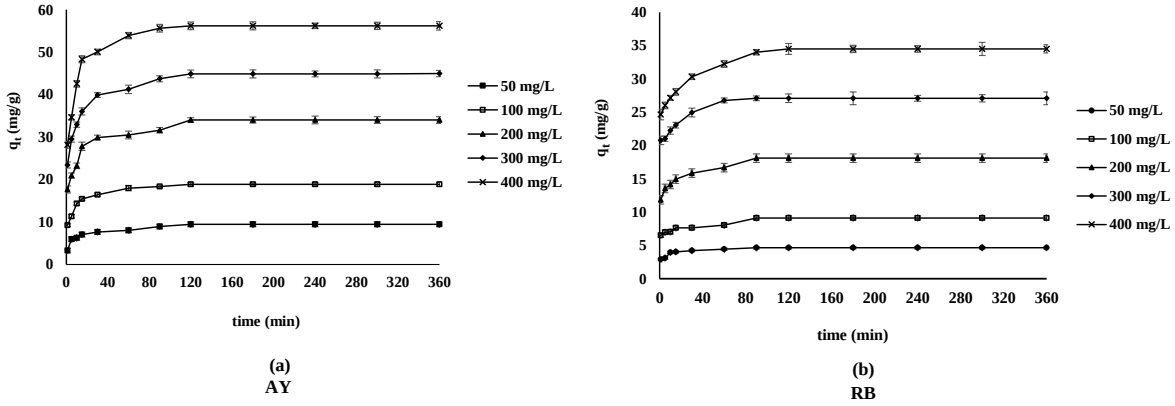

Fig. 5 Effects of contact time on dye adsorption: (a) AY and (b) RB. Conditions: pH 2, initial dye concentrations of 50–400 mg/l, and adsorbent dose of 0.5 g for AY and 1.0 g for RB, at 30 °C.

initial dye concentration on amaranth dye adsorption onto water hyacinth leaves [17] and brilliant green dye adsorption by NaOH-treated sawdust [19].

Adsorption kinetics

The pseudo-first-order, pseudo-second-order, and intraparticle diffusion models were used to analyze the kinetic adsorption data of AY and RB on the WHL. The data in Fig. 5 were tested using these 3 kinetic models, and their plots are shown in Fig. 6(a–c). Also, the calculated parameter values are tabulated in Table 2.

Based on the correlation coefficient (R^2) in Table 2, the pseudo-second-order model better fitted the kinetic data than the pseudo-first-order model and intraparticle diffusion.

At concentrations of 50–400 mg/l, the equilibrium adsorption capacity values calculated from the pseudo-second-order model (q_e, cal) were 4.675 to 34.843 mg/g for RB and 9.606 to 56.818 mg/g for AY. Furthermore, the values calculated from the pseudo-second-order equation were close to the experimental values (q_e, exp). The adsorption data were best fitted by a pseudo-second-order model, indicating that the adsorption occurred with the diffusion of the external liquid membrane, surface adsorption, and intraparticle diffusion [21]. Moreover, the adsorption initial rate constant ($h = k_2 q_e^2$) increased with increased initial concentration, revealing that the external mass transfer was the rate-controlling mechanism [25]. The adsorption results from the intraparticle diffusion plots (Fig. 6c) showed 3 linear steps for AY and 2 linear steps for RB. The first linear step represents the external film diffusion, and the following linear steps represent pore diffusion and equilibrium. The final step of the adsorption of the dyes is the equilibrium stage, where intraparticle diffusion begins to slow down due to the extremely low concentration of adsorbate remaining in the solutions [26]. In Table 2, $K_{id}(1)$ and $K_{id}(2)$ are rate parameters calculated from the slopes of the linear lines of diffusion which occurred before the beginning of equilibrium (horizontal line). They are higher for higher initial concentration, indicating that dye molecules diffuse through mesopore and micropore [27]. As the plot of intraparticle diffusion does not pass through the origin, there is a boundary layer effect [28]. This implies that intraparticle diffusion is not the sole rate-limiting step in the adsorption process [29]. Therefore, the external film diffusion and intraparticle diffusion promoted adsorption onto the WHL [30].

Equilibrium adsorption and isotherms

Adsorption equilibrium is an essential physicochemical condition for evaluating the adsorption process. The Langmuir and Freundlich isotherms were used to calculate equilibrium adsorption data for AY and RB on the WHL at different initial dye concentrations of 50–500 mg/l (50, 100, 200, 300, 400, and 500 mg/l) for AY and 50–250 mg/l (50, 100, 150, 200, and 250 mg/l) for RB at 30 °C. The linear plots of the Langmuir adsorption isotherm are shown in Fig. 7. The calculated parameters of the 2 isotherms are presented in Table 3. Based on the R^2, the equilibrium adsorption data fit the Langmuir isotherm better than the Freundlich isotherm. The maximum monolayer adsorption capacities for AY and RB adsorption were 36.63 and 23.98 mg/g, respectively. Moreover, the R_L values were in the range of 0.145–0.016 and 0.224–0.054 for the adsorption of AY and RB, respectively, indicating that the adsorption was favorable. The value of $1/n < 1$ for the Freundlich isotherm model indicated a normal Langmuir isotherm and reflected the favorable adsorption [31].

Thermodynamics of adsorption

The thermodynamic parameters of adsorption such as the Gibbs free energy change (ΔG°), enthalpy change (ΔH°), and entropy change (ΔS°) were determined.

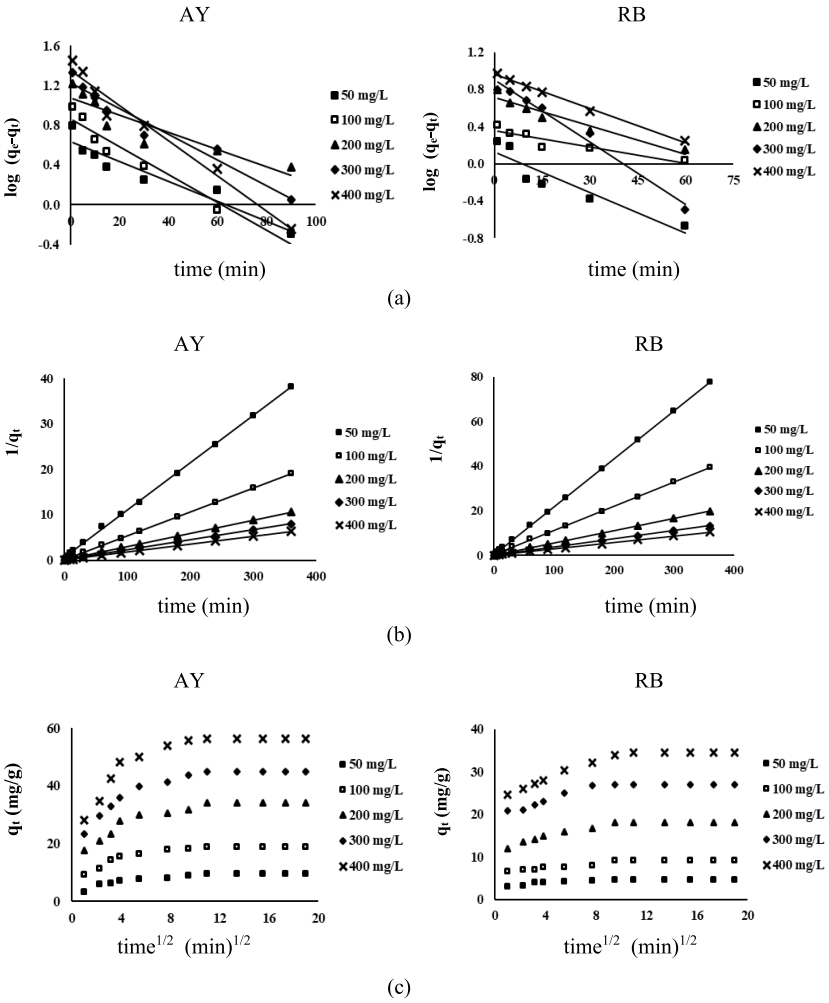

Fig. 6 Plots of kinetic models of dye adsorption at the initial concentrations of 50–400 mg/l: (a) pseudo-first order, (b) pseudo-second order, and (c) intraparticle diffusion.

Table 2 Kinetic parameters of dye adsorption on WHL.

Kinetic model	AY (mg/l)					RB (mg/l)				
	50	100	200	300	400	50	100	200	300	400
q_e (exp) (mg/g)	9.436	18.868	34.027	44.885	56.225	4.643	9.128	18.109	27.088	36.062
Pseudo-first order										
q_e (cal) (mg/g)	4.291	7.253	16.915	16.735	22.225	1.335	2.291	5.160	8.196	9.156
k_1 (min^{-1})	0.023	0.032	0.020	0.030	0.041	0.033	0.013	0.023	0.051	0.028
R^2	0.914	0.954	0.829	0.952	0.970	0.863	0.848	0.931	0.983	0.995
Pseudo-second order										
q_e (cal) (mg/g)	9.606	19.084	34.483	45.455	56.818	4.675	9.225	18.282	23.241	34.843
k_2 (g/(mg · min))	0.019	0.017	0.007	0.007	0.007	0.111	0.035	0.021	0.025	0.011
h	1.754	6.192	8.324	14.463	22.598	2.426	2.979	7.019	13.504	13.355
R^2	0.999	1.000	0.999	0.999	0.999	1.000	0.999	0.999	1.000	0.999
Intraparticle diffusion										
C1 (mg/g)	3.115	8.008	14.79 8	20.745	24.217	3.629	6.287	12.694	22.141	25.277
$K_{\text{id}}(1)$	0.924	1.696	2.892	3.690	5.252	0.106	0.271	0.553	0.545	0.913
R^2	0.859	0.921	0.954	0.976	0.914	0.996	0.928	0.950	0.908	0.997
C2 (mg/g)	5.717	13.732	21.900	32.569	48.469	–	–	–	–	–
$K_{\text{id}}(2)$	0.332	0.490	1.080	1.142	7.295	–	–	–	–	–
R^2	0.997	0.963	0.934	0.971	0.946	–	–	–	–	–

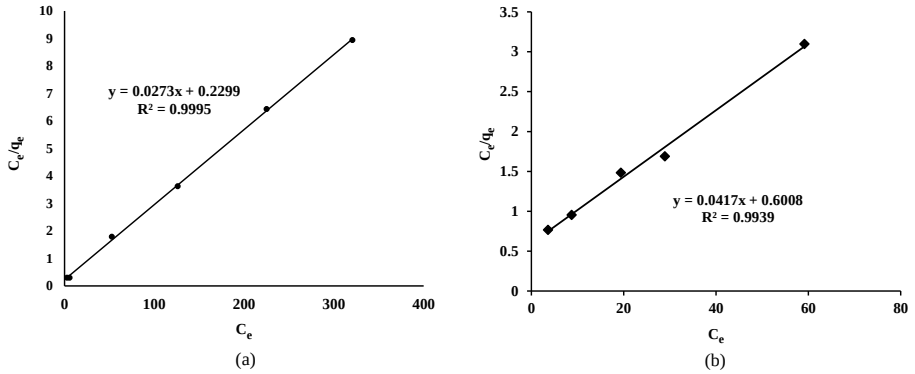

Fig. 7 Langmuir isotherm plots of (a) AY and (b) RB adsorption on WHL. Conditions: pH 2, contact time 120 min for AY and 90 min for RB, at 30 °C.

Table 3 Parameters of the adsorption isotherms on WHL.

Dye	Langmuir isotherm				Freundlich isotherm		
	$q_{\max}$ (mg/g)	K_L (l/mg)	R_L	R^2	$1/n$	K_F (mg/g)	R^2
AY	36.63	0.119	0.145–0.016	0.999	0.251	179.43	0.875
RB	23.98	0.069	0.224–0.054	0.994	0.513	9.98	0.954

The experiments were performed at equilibrium using 50 mg/l of dye solution at 20, 30, and 40 °C. At each adsorption temperature, ΔG° was calculated using Eq. (8). The graphs of ΔG° versus T were plotted and are shown in Fig. 8(a,b) for AY and RB, respectively. ΔH° and ΔS° values were determined from the intercept and slope of the graphs. The thermodynamic parameters of adsorption are shown in Table 4.

As seen in Table 4, the ΔG° values were −2.435, −2.942, and −4.315 kJ/mol for AY, while the ΔG° values were 0.740, −0.667, and −2.367 kJ/mol for RB. The value of ΔG° became more negative at higher adsorption temperatures, indicating that the adsorption process was more favorable and spontaneous due to the increased mobility of the dye molecules in the solution at higher temperatures. A similar result has been reported for the adsorption of methylene blue using biochar derived from water hyacinth [32]. The enthalpy change (ΔH°) values of adsorption were 25.24 and 46.31 kJ/mol for AY and RB, respectively.

Table 4 Thermodynamic parameters for dye adsorption at different temperatures.

Dye	Temp. (K)	ΔG° (kJ/mol)	ΔH° (kJ/mol)	ΔS° (kJ/mol · K)
AY	293	−2.435	25.24	0.094
	303	−2.942		
	313	−4.315		
RB	293	0.740	46.31	0.155
	303	−0.667		
	313	−2.367		

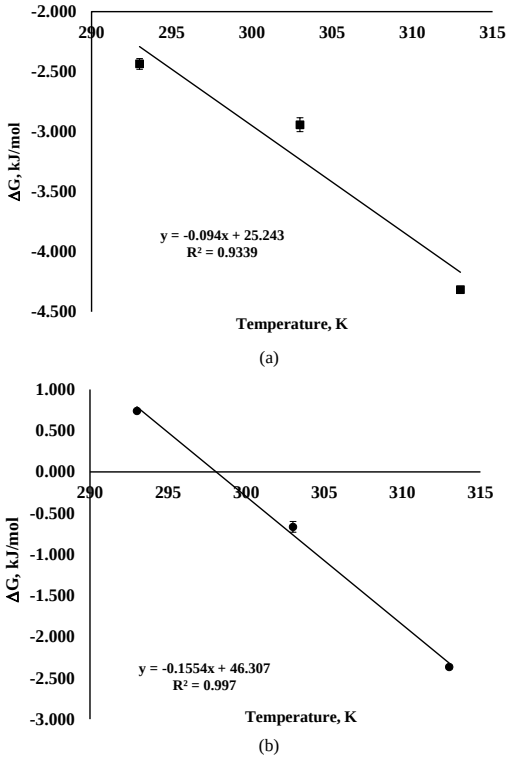

Fig. 8 Thermodynamic plots for the adsorption of (a) AY and (b) RB. Conditions: pH 2, contact time 120 min for AY and 90 min for RB, and initial concentration of 50 mg/l, at temperatures: 20, 30, and 40 °C.

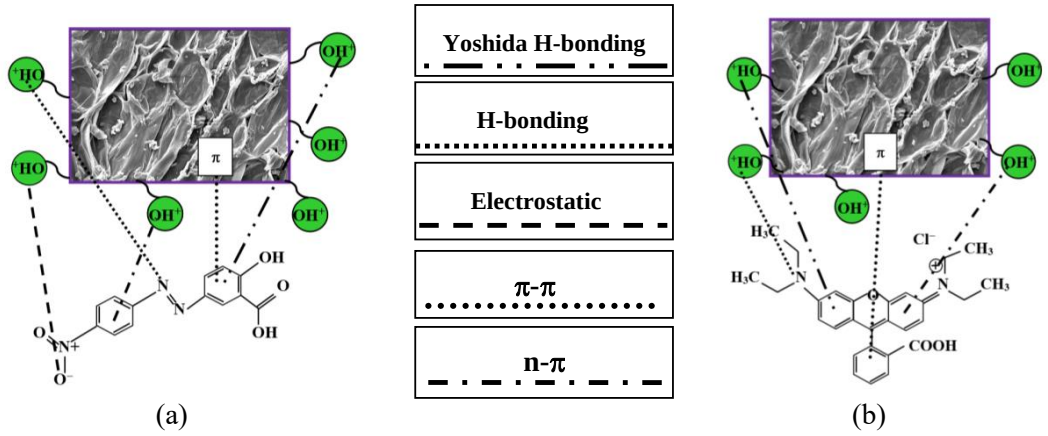

Fig. 9 Adsorption mechanisms of (a) AY and (b) RB on WHL.

The positive value of ΔH° confirmed that the dye adsorption was endothermic. Generally, the enthalpy change for physisorption is lower than 84 kJ/mol, but for chemisorption, it is 84–420 kJ/mol [33]. Therefore, the adsorption of AY and RB onto WHL can be considered physisorption, which is the dominant mechanism in the adsorption process. The entropy change (ΔS°) values of adsorption were 0.094 and 0.155 kJ/(mol·K) for AY and RB, respectively. The positive value of ΔS° suggested an increase in entropy with adsorption, which occurred due to an increase in randomness at the solid-solution interface during adsorption.

Adsorption mechanism

According to the results of FTIR spectroscopy and the adsorption experiments, the adsorption mechanisms were determined and are presented in Fig. 9. The thermodynamic study showed that the adsorption was physisorption. For the adsorption at pH 2, an electrostatic interaction (– –) formed between the negative part of the nitro group in AY and the positively-charged surface of the adsorbent ($-OH_2^+$). After adsorption, the FTIR spectra showed a decrease in the intensity of the −OH group at 3303.3 cm^{-1}, confirming the existence of dipole-dipole hydrogen bonding and Yoshida hydrogen bonding [34]. The peak of the aromatic C=C bonds decreased in intensity, confirming the contribution of the $n-\pi$ and $\pi-\pi$ interactions. The $n-\pi$ interactions might occur between the lone pair of electrons on the oxygen atoms (electron donors) at the surface of the adsorbent and the π orbitals (electron acceptors) of the aromatic rings of the dyes. The $\pi-\pi$ interactions can be formed between the π-electrons in the carbonaceous adsorbent and the π-electrons in the aromatic ring of the dye molecules [35].

CONCLUSION

The present work used water hyacinth to remove the dyes: alizarin yellow, an anionic azo dye, and rhodamine B, a highly water-soluble synthetic dye, from a preparation of aqueous extract. The removal of both dyes increased with an increase in time, dye concentration, and temperature but decreased with an increase in dye solution pH. The adsorption was endothermic and agreed well with pseudo-second-order kinetics and the Langmuir isotherm model and can be ascribed to multiple adsorption mechanisms. WHL was found to be an effective adsorbent for removing the dyes, thus having the potential to be used as a promising and low-cost adsorbent for the treatment of industrial wastewater.

Acknowledgements: The authors would like to thank Thepsatri Rajabhat University for the support of this research.

REFERENCES

1. Pathania D, Sharma S, Singh P (2017) Removal of methylene blue by adsorption onto activated carbon developed from *Ficus carica* bast. *Arab J Chem* **10**, S1445–S1451.
2. Sharma P, Kaur H (2011) Sugarcane bagasse for the removal of erythrosin B and methylene blue from aqueous waste. *Appl Water Sci* **1**, 135–145.
3. Parvin S, Hossen A, Rahman W, Hossen I, Halim A, Biswas BK, Khan AS (2019) Uptake hazardous dye from wastewater using water hyacinth as bioadsorbent. *Eur J Sustain Dev* **3**, em0065.
4. Han X, Niu X, Ma X (2012) Adsorption characteristics of methylene blue on poplar leaf in batch mode: Equilibrium, kinetics and thermodynamics. *Korean J Chem Eng* **29**, 494–502.
5. Nandi BK, Goswami A, Purkait MK (2009) Adsorption characteristics of brilliant green dye on kaolin. *J Hazard Mater* **161**, 387–395.
6. Rehman R, Mahmud T, Arshad A (2015) Removal of alizarin yellow and murexide dyes from water using

formalin treated *Pisum sativum* peels. *Asian J Chem* **27**, 1593–1598.
7. Duarte Neto JF, Pereira IDS, da Silva VC, Ferreira HC, Neves G de A, Menezes RR (2018) Study of equilibrium and kinetic adsorption of rhodamine B onto purified bentonite clays. *Ceramica* **64**, 598–607.
8. Oyekanmi AA, Ahmad A, Hossain K, Rafatullah M (2019) Adsorption of Rhodamine B dye from aqueous solution onto acid-treated banana peel: Response surface methodology, kinetics and isotherm studies. *PLoS One* **15**, e0216878.
9. Sateu D, Malutan T (2013) Adsorption of cationic dye on cellolignin. *BioResource* **8**, 427–446.
10. Hameed BH, El-Khaiary MI (2008) Malachite green adsorption by rattan sawdust: Isotherm, kinetic and mechanism modeling. *J Hazard Mater* **159**, 574–579.
11. Kumar PS, Ramalingam S, Senthamarai C, Niranjanaa M, Vijayalakshmi P, Sivanesan S (2010) Adsorption of dye from aqueous solution by cashew nut shell: studies on equilibrium isotherm, kinetics and thermodynamics of interactions. *Desalination* **261**, 52–60.
12. Khan MMR, Ray M, Guha AK (2011) Mechanistic studies on the binding of Acid Yellow 99 on coir pith. *Bioresour Technol* **102**, 2394–2399.
13. Lim LBL, Priyantha N, Tennakoon DTB, Chieng HL, Dahri MK, Suklueng M (2017) Breadnut peel as a highly effective low-cost biosorbent for methylene blue: Equilibrium, thermodynamic and kinetic studies. *Arab J Chem* **10**, S3216–S3228.
14. Keereerak A, Chinpa W (2020) A potential biosorbent from *Moringa oleifera* pod husk for crystal violet: Kinetics, isotherms, thermodynamic and desorption studies. *ScienceAsia* **46**, 186–194.
15. Low KS, Leek CK, Tan K (1995) Biosorption of basic dyes by water hyacinth roots. *Bioresour Technol* **52**, 79–83.
16. Tarawou T, Horsfall Jr M, Vicente JL (2007) Adsorption of Methyl Red by water-hyacinth (*Eichornia crassipes*) biomass *Chem Biodivers* **4**, 2236–2245.
17. Guerrero-Coronilla I, Morales-Barrera L, Cristiani-Urbina E (2015) Kinetic, isotherm and thermodynamic studies of amaranth dye biosorption from aqueous solution onto water hyacinth leaves. *J Environ* **152**, 99–108.
18. Guerrero-Coronilla I, Aranda-Garcia E, Cristiani-Urbina E (2019) Biosorption of metanil yellow dye from aqueous solutions by the entire water hyacinth plant (*Eichhornia crassipes*) and its vegetative organs. *Environ Eng Manag* **18**, 1671–1682.
19. Mane VS, Babu PVV (2011) Studies on the adsorption of Brilliant Green dye from aqueous solution on to low-cost NaOH treated sawdust. *Desalination* **273**, 321–329.
20. Adekola FA, Hodonou DSS, Adegoke HI (2007) Thermodynamic and kinetic studies of biosorption of iron and manganese from aqueous medium using rice husk ash. *Appl Water Sci* **6**, 319–330.
21. Zhu Y, Yi B, Yuan Q, Wu Y, Wang M, Yan S (2018) Removal of methylene blue from aqueous solution by cattle manure-derived low temperature biochar. *RSC Adv* **8**, 19917–19929.
22. Bopat SA, Jaspal DK (2020) Surface-modified water hyacinth (*Eichhornia crassipes*) over activated carbon for wastewater treatment: A comparative account. *S Afr J Chem* **72**, 70–80.
23. Kumar A, Negi YS, Choudhary V, Bhardwaj NK (2014) Characterization of cellulose nanocrystals produced by acid-hydrolysis from sugarcane bagasse as agro-waste. *J Mater Phys Chem* **2**, 1–8.
24. Gad HMH, El-Sayed A (2009) Activated carbon from agricultural by-products for the removal of Rhodamine-B from aqueous solution. *J Hazard Mater* **168**, 1070–1081.
25. Omorogie MO, Babalola JO, Unuabonah EI, Song W, Gong JR (2016) Efficient chromium abstraction from aqueous solution using a low-cost biosorbent: *Nauclea diderrichi* seed biomass waste. *J Saudi Chem Soc* **20**, 49–57.
26. Nethaji S, Sivasamy A, Mandal AB (2013) Adsorption isotherms, kinetics and mechanism for the adsorption of cationic and anionic dyes onto carbonaceous particles prepared from *Juglans regia* shell biomass. *Int J Environ Sci Technol* **10**, 231–242.
27. Lakshmi UR, Srivastava VC, Mall ID, Lataye DH (2009) Rice husk ash as an effective adsorbent: evaluation of adsorptive characteristics for indigo carmine dye. *J Environ Manage* **90**, 710–720.
28. Zulfikar MA, Setiyanto H, Djajanti SD (2013) Effect of temperature and kinetic modelling of lignosulfonate adsorption onto powdered eggshell in batch systems. *Songklanakarin J Sci Technol* **35**, 309–316.
29. Zhou X, Xu M, Wang L, Liu X (2019) The adsorption of methylene blue by an amphiphilic block copoly(arylene ether nitrile) microsphere-based adsorbent: Kinetic, isotherm, thermodynamic and mechanistic studies. *J Nanomater* **9**, 1356.
30. Pan M, Lin X, Xie J, Huang X (2017) Kinetic, equilibrium and thermodynamic studies for phosphate adsorption on aluminum hydroxide modified palygorskite nanocomposites. *RSC Adv* **7**, 4492–4500.
31. Kaur S, Rani S, Mahajan RK (2013) Adsorption kinetics for the removal of hazardous dye congo red by biowaste materials as adsorbents. *J Chem* **2013**, 628582.
32. Xu Y, Liu Y, Liu S, Tan X, Zeng G, Zeng W, Ding Y, Cao W, et al (2016) Enhanced adsorption of methylene blue by citric acid modification of biochar derived from water hyacinth (*Eichornia crassipes*). *Environ Sci Pollut Res* **23**, 23606–23618.
33. Palanisamy PN, Agalya A, Sivakumar P (2013) Polypyrrole composite – A potential material for the removal of acid dyes. *Asian J Chem* **25**, 5891–5896.
34. Grabi H, Derridj F, Lemlikchi W, Guenin E (2021) Studies of the potential of a native natural biosorbent for the elimination of an anionic textile dye Cibacron Blue in aqueous solution. *Sci Rep* **11**, 9705.
35. Tran HN, You S-J, Choa H-P (2017) Insight into adsorption mechanism of cationic dye onto agricultural residues-derived hydrochars: Negligible role of $\pi - \pi$ interaction. *Korean J Chem* **34**, 1708–1720.